Effect of Imperfect Direct Simple Shear Test Boundary Conditions on Calibration of Constitutive Models

Daniel Wai & Mathan V. Manmatharajan
Department of Civil & Mining Engineering – University of Toronto, Toronto, Ontario, Canada
Thamer Yacoub
Rocscience Inc., Toronto, Ontario, Canada
Mason Ghafghazi
Department of Civil & Mining Engineering – University of Toronto, Toronto, Ontario, Canada

ABSTRACT
The direct simple shear (DSS) test is commonly used to calibrate constitutive models for various geotechnical problems. However, constitutive models are calibrated under the assumption of *ideal* simple shear stress conditions even though this is not achieved in the DSS test. Near frictionless vertical boundaries that enforce lateral confinement are not capable of inducing complementary shear stresses necessary for simple shear stress conditions. The effect of friction between the soil and vertical boundaries on stress distribution is not well studied and may impact the calibration of constitutive models. Undrained monotonic simple shear tests considering soil-ring interaction are simulated using finite element analyses. Simulations of the expected soil-ring friction compare well with *ideal* simple shear results despite stress non-uniformities near the vertical boundaries. Although higher soil-ring friction reduces stress non-uniformities during shearing, the friction develops stress non-uniformities during the consolidation phase that cannot be ignored when calibrating models.

RÉSUMÉ
L'essai cyclique en cisaillement simple est couramment utilisé afin de calibrer des modèles constitutifs. Toutefois, ces modèles constitutifs sont calibrés en assumant des conditions idéales de cisaillement simple qui ne se produisent pas lors de l'essai. Aucune force de cisaillement complémentaire n'est présente aux limites verticales de l'appareil qui restreignent l'expansion latérale de l'échantillon. Ces forces de cisaillement doivent exister dans des conditions idéales de cisaillement simple. Le frottement entre l'échantillon de sol et les limites verticales a un impact sur la distribution des contraintes qui n'est pas suffisamment étudié, alors que ce frottement pourrait influencer la calibration de modèles constitutifs. Dans la présente étude, des essais en cisaillement simple monotoniques non-drainés sont simulés à l'aide de modèles à éléments finis. Les résultats des simulations sont comparables à des conditions idéales de cisaillement simple même si le frottement entre le sol et les limites verticales cause des contraintes non-uniformes. Un frottement élevé entre le sol et les limites verticales réduit l'ampleur des contraintes non-uniformes. Toutefois, le frottement créé lors de l'étape de consolidation ne peut pas être ignoré lors de la calibration de modèles constitutifs.

1 INTRODUCTION

Numerical modelling is becoming increasingly popular in analyzing geotechnical problems due to constant improvements in computational ability and the industry's move towards more sophisticated and deformation based design methods. Simulations can consider complex site conditions and soil behaviour using finite element analysis (FEA) software such as RS3 (Rocscience Inc. 2019) or FLAC3D (ITASCA Consulting Group Inc. 2019). These software packages require advanced constitutive models to capture soil stress-strain response in a realistic manner. Numerical modelling cannot obtain useful results without accurate calibration of constitutive models against laboratory tests. It becomes essential that laboratory tests reflect or at least closely approximate assumed stress conditions when deriving model parameters.

The direct simple shear (DSS) test is commonly used to calibrate constitutive models for soil under simple shear loading. Specimens are consolidated by a vertical stress before a shear load is applied to the base pedestal, as shown in Figure 1. To apply *ideal* simple shear conditions, the boundaries must allow for development of the shear stresses shown in Figure 2(a). During shearing, opposite sides must remain parallel. DSS tests accomplish this by allowing rotation (tilting) of vertical boundaries during shear loading but ensuring no rotation of the top cap or base pedestal. Vertical boundaries must also ensure no change in cross-sectional area. For undrained tests, no height change may occur to satisfy the constant volume condition.

Many DSS testing apparatuses have been developed over the years. The Royal Swedish Geotechnical Institute (SGI) device, first built in 1936, applied simple shear loading on a cylindrical soil specimen (Kjellman 1951). The specimen was contained in a rubber membrane that was laterally confined by a stack of stiff rings to ensure no change in diameter. The Norwegian Geotechnical Institute (NGI) device was a modification of the SGI device that achieved lateral confinement using a wire reinforced rubber membrane instead of stacked rings (Bjerrum and Landva 1966). The Cambridge device applied simple shear loading on a cuboid soil specimen that was laterally confined by hinged vertical stiff plates (Roscoe 1953). Instead of stiff lateral boundaries that enforced constant cross-sectional area, the University of Western Australia (UWA)(Mao and Fahey 2003) and the University of California at Berkeley

(Villet et al. 1985) used devices that applied constant total lateral stress by conducting the DSS test on a cylindrical specimen within a pressure cell.

Current DSS testing apparatuses cannot impose *ideal* simple shear conditions which is assumed for the calibration of constitutive models. DSS tests typically impose near frictionless vertical boundaries due to the inability of the stacked rings and membrane setup to transfer the vertical friction force. The vertical frictionless boundary is necessary to avoid stress shedding during the consolidation phase. However, as illustrated in Figure 2(b), the near-frictionless vertical boundaries do not allow development of complementary shear stresses necessary for *ideal* simple shear conditions (Airey et al. 1985; Lucks et al. 1972; Roscoe 1953; Saada and Townsend 1981). Lacking complementary frictional forces in the simple shear test creates a mechanically impossible stress field for a single element meaning that either the element will have rotational acceleration, or a Mohr circle cannot describe its static equilibrium. Many numerical solutions have been developed to study imperfect boundary effects and estimate the development of stress non-uniformities (Doherty and Fahey 2011; Lucks et al. 1972; Roscoe 1953; Saada and Townsend 1981; Shen et al. 1978). In these studies, the assumed contact behaviour between the soil and vertical boundaries is unclear. The effect of soil-ring friction on DSS testing has not been well studied and may impact the calibration of constitutive models. Higher contact friction allows better development of complementary shear stresses but may induce stress non-uniformities during the consolidation phase. Bernhardt et al. (2016) showed from a study of steel spheres in a DSS apparatus that higher steel spheres to ring friction resulted in more strain hardening and dilative response. Their results suggest that higher soil-ring friction can potentially overestimate shear strength properties.

This paper summarizes an investigation into the effect of soil-ring friction in an SGI type device on the calibration of constitutive models. Figure 1 shows schematics of a soil specimen in an SGI device. The soil-ring interaction is studied through three-dimensional (3D) finite element analysis (FEA) of undrained monotonic simple shear tests using the software ABAQUS (Dassault Systèmes 2012). The soil stress-strain behaviour is captured using the constitutive model SANISAND for its ability to capture sand plasticity during both monotonic and cyclic shear loading (Dafalias and Manzari 2004). The simulation models the stacked rings confining a typical cylindrical soil specimen. The model is calibrated using triaxial and simple shear test data of a poorly graded medium sand. A parametric study was performed to investigate the interaction of soil-ring friction angles and soil densities. The study analyzes simulations using the minimum and maximum expected soil-ring friction in the laboratory in addition to the soil-ring friction necessary to achieve ideal simple shear conditions.

2 BACKGROUND

Numerical solutions have been developed to study boundary effects on stress concentration in simple shear

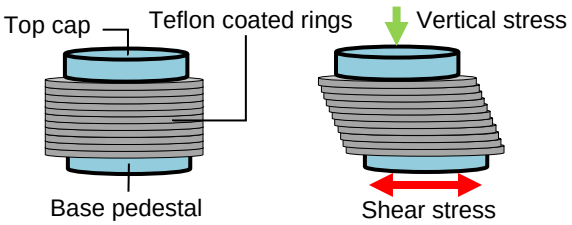

Figure 1. Typical SGI simple shear test boundaries

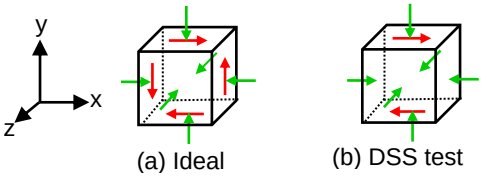

Figure 2. Simple shear stress state

tests. Roscoe (1953) used a mathematical stress function that qualitatively showed shear and vertical stress concentrations around the edges of a specimen in a Cambridge type device. The results agreed with a study of boundary effects in a NGI type device using 3D linear elastic FEA by Luck et al. (1972). They reported that approximately 70% of the total area around the specimen core has a uniform stress distribution. Saada and Townsend (1981) did not agree with the previous numerical analyses of the Cambridge and NGI type devices and argued that the assumed boundary conditions, especially at the vertical boundaries, were physically impossible to impose by the devices. Shen et al. (1978) also conducted 3D linear elastic FEA of the NGI type device and provided recommendations to improve the uniformity of shear strain distribution. Doherty and Fahey (2011) then modelled a UWA type device using 3D non-linear FEA to better capture real soil response and showed that stress non-uniformities may underestimate shear strength.

There have not been many studies on the effect of soil-ring friction. In many numerical analyses, the assumed contact behaviour between the soil and vertical boundaries is unclear (Lucks et al. 1972; Roscoe 1953; Saada and Townsend 1981; Shen et al. 1978). The UWA type device that was modelled by Doherty and Fahey (2011) could not develop significant complementary shear stresses due to its design. Bernhardt et al. (2016) and Chang et al. (2016) considered soil-ring friction in their study of boundary effects in the DSS device using Distinct Element Method (DEM) analyses. The results were interpreted qualitatively as the simulations were calibrated using DSS tests of steel spheres instead of soil. Bernhardt et al. (2016) studied the effects of soil-ring friction on stress-strain response in the SGI device using 3D DEM. They showed that higher steel spheres to ring friction resulted in more strain hardening and dilative response. Their results suggest that higher soil-ring friction can potentially overestimate shear strength properties. Chang et al. (2016) compared boundary effects of the SGI and Cambridge type devices using 2D DEM that considered soil to vertical boundary friction. The results showed no significant differences between SGI and Cambridge type model results which implies that the effect

of soil-ring friction should be similar for both devices. Bernhardt et al. (2016) and Chang et al. (2016) provided useful insights on the potential effects of soil-ring friction on stress-strain response, but did not perform parametric studies on the effects of soil-ring frictions expected in practice and compare them to *ideal* simple shear conditions. Previous studies can be improved in the study of contact friction between soil and rings on the stress-strain response observed.

3 MODELLING OF SIMPLE SHEAR TEST

3.1 Soil Constitutive Model

Soil stress-strain behaviour is captured using the Simple ANIsotropic SAND (SANISAND) model formulated by Dafalias and Manzari (2004). The bounding surface model primarily captures sand plasticity due to changes in stress ratio (η) which occur continuously during simple shear tests. Figure 3 shows the triaxial space representation of the formulation. The model uses a thin, open-ended wedge yield surface fixed at the origin. The model incorporates a rotational hardening parameter (α) to model sand plasticity behaviour. The size of the wedge is based on a thickness parameter (m) and defines the region of elastic behaviour. The thin wedge and rotational hardening parameter are ideal for capturing sand plasticity during load reversal, such as during cyclic shear loading. The model requires fifteen parameters that can be categorized according to their use in equations of elasticity, critical state, yield surface, plastic modulus, dilatancy and fabric-dilatancy. Masin et al. (2018) implemented SANISAND in a user-defined material model (UMAT) file that can be used in ABAQUS simulations. The UMAT file is publicly available from the database of the SoilModels project, previously known as the soilmodels.info project, founded by Gudehus et al. (2008). The UMAT's numerical stability was improved by adjustments to the convergence criteria and it was verified by comparison to simulation results by Dafalias and Manzari (2004).

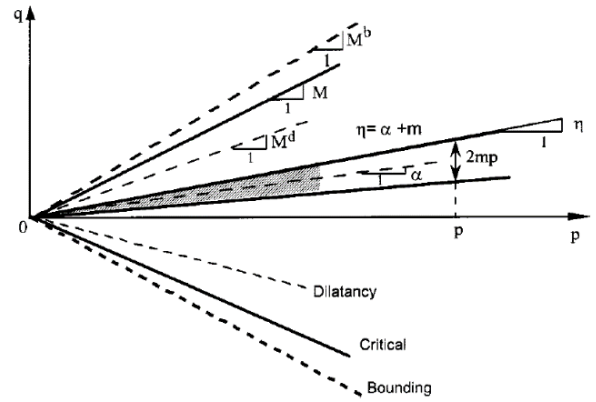

Figure 3. Illustration of the yield, critical state, dilatancy and bounding lines in deviator stress (q), mean effective stress (p) space (from Dafalias and Manzari 2004)

3.2 Calibration

Drained triaxial and undrained DSS tests are conducted on poorly graded medium sand using a SGI type device at the University of Toronto. The sand is sourced from the Hutcheson quarry located near Huntsville, Ontario and is referred to as Hutcheson sand. The mineral composition is comprised of quartz, feldspar, amphiboles and minor amounts of other minerals. The particle size distribution median diameter (D_{50}) is 0.46 mm and the uniformity coefficient (C_u) is 2.42 . A gradation of 60% medium sand and 40% fine sand is used in the study. The soil maximum and minimum void ratios are 0.877 and 0.602 respectively. The simulations model low relative density (D_r= 24%) specimens with a state parameter (ψ) of 0.025, and high relative density (D_r= 146%) specimens with a state parameter (ψ) of -0.31. The device uses Teflon coated stacked rings to apply lateral confinement on a 63.5 mm diameter by approximately 20 mm height cylindrical soil specimen that is encased in a rubber membrane. Teflon is a friction reducer that minimizes friction among the rings. The soil constitutive model is calibrated using experimental data by simulating a single element model under *ideal* simple shear conditions which is explained in detail later. Interpretation of drained triaxial tests established an initial set of parameters using the approach by Taiebat and Dafalias (2008). Parameters were then adjusted based on undrained monotonic simple shear tests. Initial and adjusted parameters are presented in Table 1. Figure 4 presents the (a) shear stress vs. strain and (b) stress path plots for a sample calibrated undrained monotonic shear test. The critical state line (CSL) at the constant volume friction angle (ϕ'_{cv}) is also plotted with the stress path. Experimental and simulation results compare well.

Table 1. SANISAND calibrated model parameters

Parameter Type	Variable[1]	Value from Triaxial Data	Value from Simple Shear Data
Elasticity	G_o	75	30
	ν	0.2	0.2
Critical state	M_{tc}	1.23	1.23
	c	0.715	0.715
	λ_c	0.023	0.023
	e_o	0.81	0.81
	ξ	0.7	0.7
Yield surface	m	0.01	0.01
Plastic modulus	h_o	8.5	8.5
	c_h	0.7	0.7
	n_b	7.0	1.0
Dilatancy	A_o	0.75	0.34
	n_d	3.2	3.2
Fabric-dilatancy tensor	z_{max}	4.0	4.0
	c_z	600	600

[1]Variables (unit-less) defined by Dafalias and Manzari (2004).

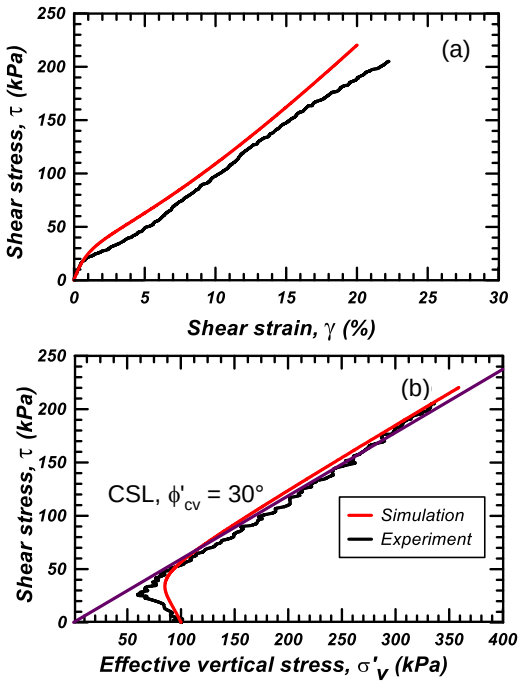

Figure 4. Sample calibrated undrained monotonic simple shear test

3.3 Finite Element Model

3.3.1 Geometry

The simulation models a typical 63.5 mm diameter by 20 mm height soil specimen using the finite element analysis software (FEA) package ABAQUS (Dassault Systèmes 2012). The cylindrical specimen is subjected to unidirectional simple shear loading which results in symmetric stress-strain distribution with respect to a vertical cut at the centre that is parallel to the shearing direction. The half-cylinder model shown in Figure 5 takes advantage of symmetry in geometry and loads to improve computation speed by reducing the required number of elements. 20 rigid rings of 1 mm height around the specimen maintain constant diameter. The mesh consists of 5820 8-noded linear isoparametric soil elements and 1600 4-noded rigid plate elements for the rings.

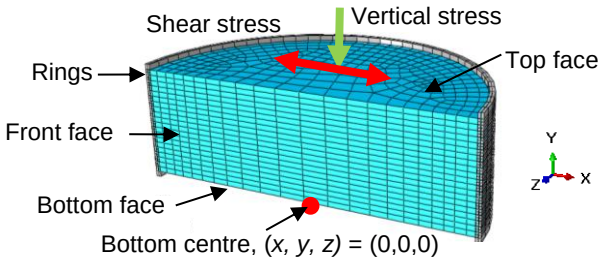

Figure 5. Finite element model of the DSS test

3.3.2 Soil-Ring Interaction

Each ring moves due to soil movement as a rigid body. A linear friction model captures the contact behaviour between the soil and the rings, as shown in Equations 1 and 2. The contact frictional stress ($\tau_{soil-ring}$) is based on the normal contact pressure ($\sigma_{soil-ring}$) and the soil-ring friction angle ($\delta_{soil-ring}$). The contact pressure is computed by the soil-ring normal stiffness ($k_{soil-ring,n}$) and compression of soil against the ring ($d_{soil-ring}$).

$$\tau_{soil-ring} = \sigma_{soil-ring} \tan \delta_{soil-ring} \quad [1]$$

$$\sigma_{soil-ring} = k_{soil-ring,n}\, d_{soil-ring} \quad [2]$$

ABAQUS automatically assigns the soil-ring normal stiffness to be much larger than the adjacent soil element stiffness and employs the Augmented Lagrange method to ensure each ring acts as a rigid boundary that displaces horizontally during shear loading (Dassault Systèmes 2012).

3.3.3 Loading and Boundary Conditions

In all loading phases, the bottom face of the model is restrained from *x* (horizontal shear direction), *y* (vertical) and *z* (out of plane) displacements (see Figure 5) and the front face is restrained from out of plane displacements. Rings are only in contact with the soil and can displace horizontally in the direction of applied shear. The simulation follows two loading phases: In the first phase, the model is consolidated by a vertical stress and the top face is restrained from lateral displacement (*x* and *z*). In the second phase, a shear strain is applied to the top face and the top is restrained from out of plane and vertical displacement to implement unidirectional constant volume test conditions.

3.3.4 *Ideal* Simple Shear Conditions

As mentioned earlier, to apply *ideal* simple shear conditions, the boundaries must allow for development of the shear stresses as shown in Figure 2(a). During shearing, opposite sides must remain parallel. Vertical boundaries must also ensure no change in cross-sectional area. For undrained tests, no height change may occur to satisfy the constant volume condition. For undrained monotonic simple shear tests under *ideal* conditions, the specimens are consolidated by a vertical stress constraining lateral strains. Then shear loading is applied constraining all strains except shear in the direction of loading.

Ideal simple shear conditions are achieved using two methods: The first method uses a single element model which assumes perfect simple shear conditions. Simulations are conducted using a single element testing software "Incremental Driver" (Niemunis 2017). The Incremental Driver's simplicity allows it to be more computationally efficient than ABAQUS for single element

models under *ideal* simple shear conditions. The second method works by applying different soil-ring friction angles during each loading phase of the multi-element SGI type stacked ring simulation in ABAQUS that is shown in Figure 5. Frictionless boundaries are set during the consolidation phase to ensure uniformly distributed stresses. Conversely, no slip conditions are set during the shearing phase to develop the necessary complementary shear stresses for *ideal* simple shear conditions. The two models produce practically identical results, so the single element model is used to produce *ideal* simple shear condition due to its efficiency. The single element model was also used for model calibration.

3.3.5 Analysis

The parametric study considers soil-ring friction of 0, 5 and 30 degrees (°). The soil-ring friction angle is assumed to be constant to study the effect of friction throughout the DSS test. The friction angles account for a combination of Teflon coated rings and rubber membrane sliding against soil. Tatsuoka and Haibara (1985) studied the interface friction angle between a Teflon sheet and air-pluviated Toyoura sand. For a Teflon sheet that is fixed on both sides, the friction angle is around 7°. However, the DSS device encases soil within a rubber membrane which compresses during consolidation from vertical stress and flexes during shearing to maintain shear deformation. The flexibility of rubber does not allow significant development of complementary shear stresses. Furthermore, the Teflon coated rings are not fixed at either end and their light weight should not be able to resist much upward complementary shear stresses. Under these conditions, the study assumes the range of achievable friction angle in the laboratory is between 0 and 5°. The lower range of 0° represents typical assumptions of frictionless boundaries. The upper range of 5° represents maximum achievable friction angle from current laboratory conditions. The ultimate friction angle of 30° represents a no slip condition between rings and soil that is necessary for *ideal* simple shear conditions in the multi-element simulation using ABAQUS. The results are compared to *ideal* simple shear conditions.

4 RESULTS AND DISCUSSION

4.1 Consolidation

Soil-ring friction affects stress non-uniformities that develop during the consolidation phase. The soil specimen is consolidated by a 100 kPa vertical stress that is in theory uniformly distributed throughout the specimen. Results are similar for low and high relative density specimens, so only the low relative density results are presented here. Figure 6 presents the shear and vertical stress distribution based on the average stress of the elements along the top and sides of the specimen at the centre cross section. As shown in Figure 6(a) and (b), higher soil-ring friction increases shear stresses near the boundaries. As a result, vertical stress concentrations develop at the top and bottom edges, as shown in Figure 6(c) and 7, to maintain uniform axial displacement imposed by the stiff top cap and bottom pedestal. Near the middle, shear stresses are zero and

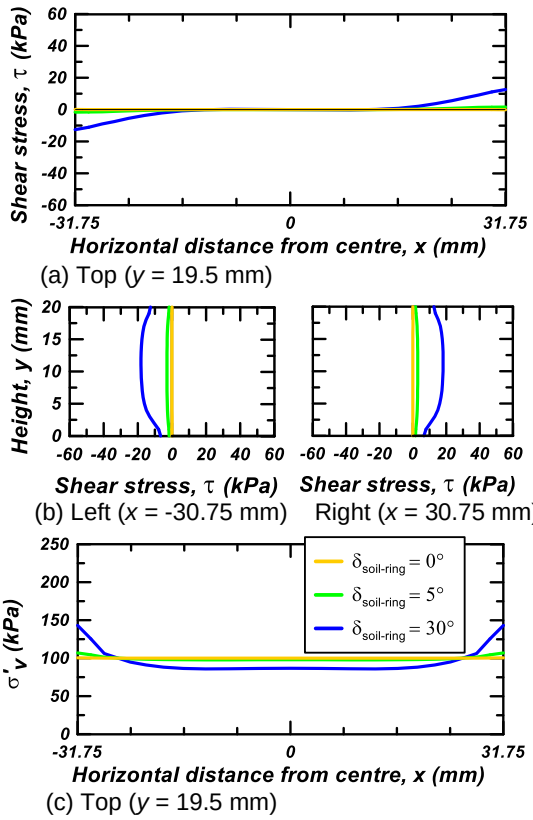

Figure 6. End of consolidation stress distribution for the centre cross section of the specimen (z = 0 mm)

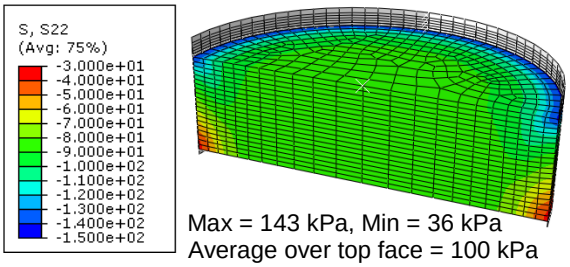

Figure 7. End of consolidation vertical effective stress contours of low relative density specimen for no slip condition, soil-ring friction angle of 30°

vertical stresses are uniformly distributed as shown in Figure 6(a) and (c). Since the average vertical stress over the top area must equal the 100 kPa stress that is applied, higher vertical stress concentrations at the top edges decreases the vertical stress of the top middle area as shown in Figure 6(c). For frictionless vertical boundaries (0°), vertical stress is 100 kPa throughout the specimen.

4.2 Monotonic Simple Shear

Soil-ring friction affects stress non-uniformities that develop during the shearing phase. Low and high relative density specimens were sheared until the simulation reached

non-convergence or 20% shear strain. The low and high relative density simulations reached non-convergence at 4% and 6% shear strain, respectively. Figure 8 presents the shear and vertical stress contours of the low relative density simulation at 4% shear strain which approximates the peak shear stress for frictionless vertical boundaries. As seen in Figure 8(a), frictionless vertical boundaries cannot develop significant complementary shear stresses. As such, maximum shear stress and vertical stress are concentrated at the top and bottom edges of the specimen as shown in Figure 8(a) and Figure 8(b). Stresses near the centre are uniformly distributed. As shown in Figure 8(a), shear stresses adjacent to the frictionless vertical boundaries quickly go from zero to the applied shear stress level. Figure 9 presents the shear and vertical stress distribution based on the average stress of elements along the top and sides of the specimen at the centre cross section. Figure 9(b) shows that complementary shear stresses develop immediately adjacent to the frictionless vertical boundaries which results in a sharp shear stress gradient that transitions to uniformly distributed stresses near the centre, as shown in Figure 8(b). Higher soil-ring friction increases complementary shear stresses near the vertical boundaries that improve stress uniformity as shown in the shear stress distribution, Figure 9(a) and (b), and in the vertical stress distribution, Figure 9(c). Thus, higher soil-ring friction improves stress uniformity in the specimen due to the development of complementary shear stresses. However, stress concentrations exist for all soil-ring friction angles as shown in Figure 8 and Figure 9. Convergence criteria becomes more difficult to satisfy with large stress concentrations at high shear strain which may have contributed to non-convergence of the simulations before the target 20% shear strain.

Soil-ring friction affects the average stress-strain response during the shearing phase. Figure 10 and Figure 11 present the shear stress vs. strain and stress path plots for low and high relative density simulations. The critical state line (CSL) at the constant volume friction angle (ϕ'_{cv}) is also plotted with the stress paths. For the multi-element stacked ring simulations, the plots present the average stress and strain values over the top area. As shown in Figure 10(a) and (b), higher soil-ring friction underestimates the average shear stress for low relative density simulations when compared to the single element *ideal* simple shear simulation. For the expected achievable range of soil-ring friction between 0 to 5°, low relative density results compare well with the *ideal* simple shear simulation. Additionally, as shown in Figure 11(a) and (b), high relative density simulations compare well with the *ideal* simple shear simulation for all tested soil-ring friction angles. Thus, the effect of soil-ring friction (or lack thereof) is negligible for typical DSS testing conditions. Higher soil-ring friction does not improve the average stress-strain response in simulating *ideal* simple shear conditions. The stress-strain response measured from DSS testing is reasonable in approximating *ideal* simple shear conditions for the calibration of constitutive models.

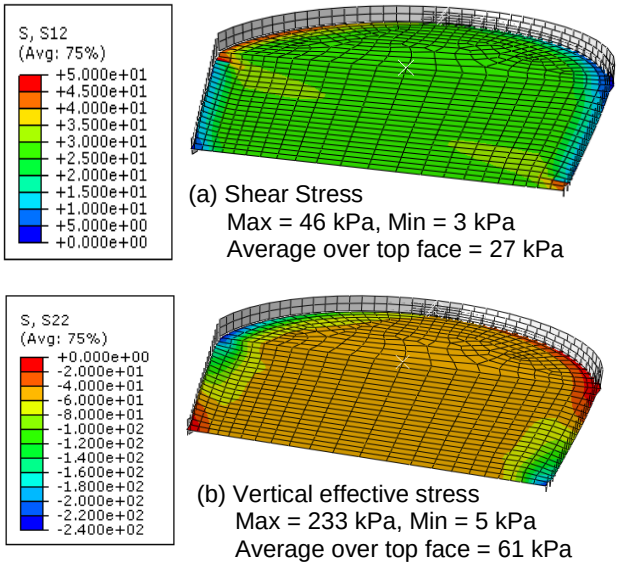

(a) Shear Stress
Max = 46 kPa, Min = 3 kPa
Average over top face = 27 kPa

(b) Vertical effective stress
Max = 233 kPa, Min = 5 kPa
Average over top face = 61 kPa

Figure 8. Stress contours of low relative density specimen at 4% shear strain for frictionless vertical boundaries, soil-ring friction angle of 0°

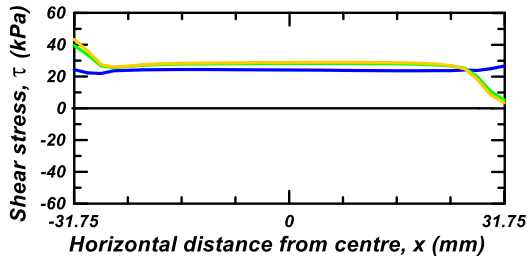

(a) Top (y = 19.5 mm)

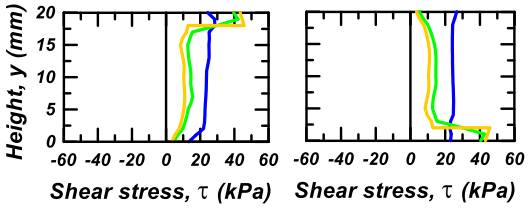

(b) Left (x = -30.75 mm) Right (x = 30.75 mm)

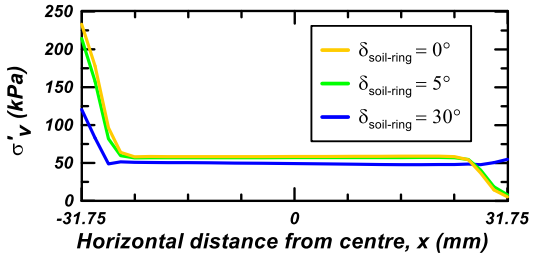

(c) Top (y = 19.5 mm)

Figure 9. Stress distribution of low relative density specimen at 4% shear strain for the centre cross section of the specimen (z = 0 mm)

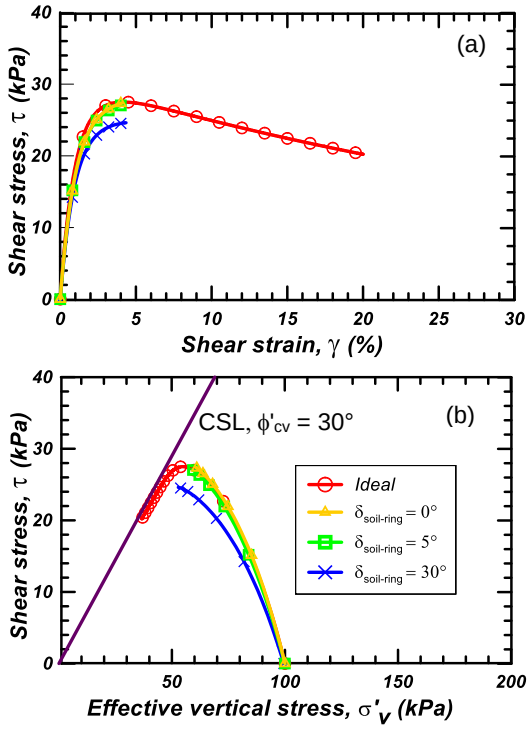

Figure 10. Monotonic test results of low relative density specimen for varying soil-ring friction angle

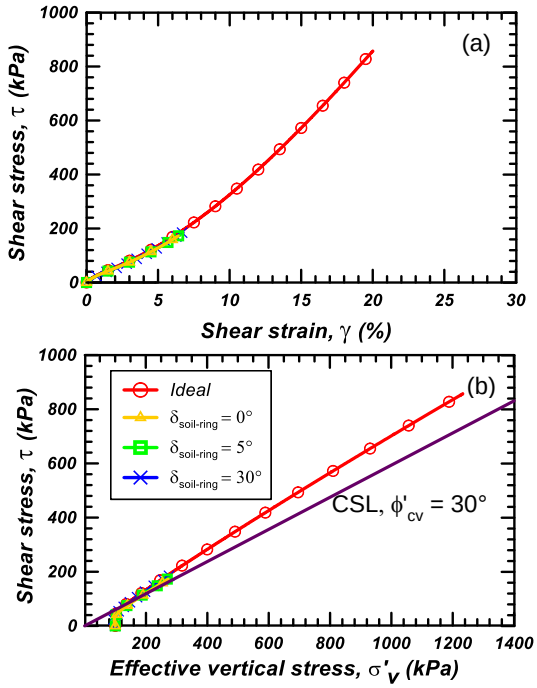

Figure 11. Monotonic test results of high relative density specimen for varying soil-ring friction angle

Stress non-uniformities that develop during the consolidation phase due to soil-ring friction, especially for $\delta_{soil-ring}$= 30°, affect the average stress-strain response during the shearing phase. As mentioned previously, Figure 6 shows that higher soil-ring friction increases shear stress and vertical stress concentrations around the specimen edges during the consolidation phase. To study the effect of soil-ring friction on the shearing phase only, frictionless vertical boundaries are set during the consolidation phase ($\delta_{soil-ring,c}$= 0°) to ensure uniform stress distribution. The soil-ring friction angle is varied for the shearing phase only. Figure 12 presents the shear stress vs. strain and stress path plots for simulations of frictionless ($\delta_{soil-ring,s}$= 0°) and no slip ($\delta_{soil-ring,s}$= 30°) vertical boundaries during the shearing phase. The critical state line (CSL) at the constant volume friction angle (ϕ'_{cv}) is also plotted with the stress paths like before. As mentioned previously, applying frictionless vertical boundaries during the consolidation phase and no slip vertical boundaries ($\delta_{soil-ring,s}$= 30°) during the shearing phase simulates *ideal* simple shear conditions. The shear stress vs. strain plot in Figure 12(a), and the stress path plot in Figure 12(b) show that varying the soil-ring friction during the shearing phase does not affect the average stress-strain response. Both soil-ring friction conditions compare well with the single element *ideal* simple shear simulation. Hence, the average stress-strain response during the shearing phase is primarily affected by the development of stress concentrations during the consolidation phase. Higher soil-ring friction increases stress concentrations during the consolidation phase that results in underestimation of shear stress during the shearing phase, as previously shown in Figure 10.

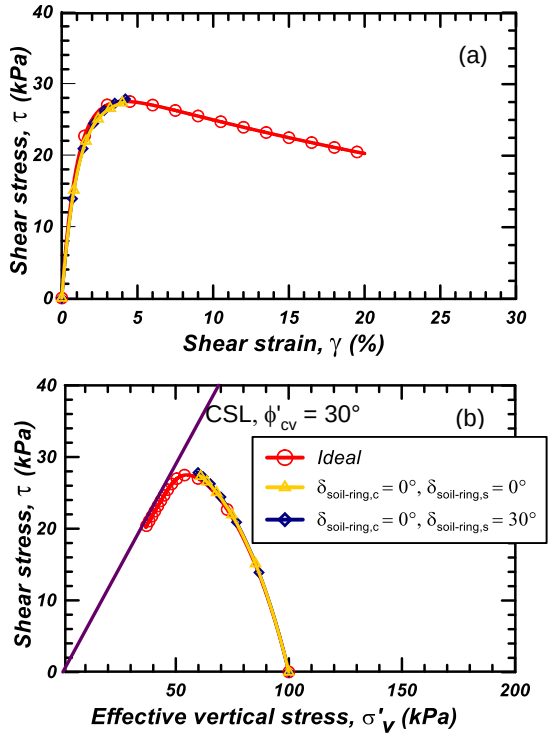

Figure 12. Monotonic test results of low relative density varying soil-ring friction angle during shearing phase only

5 CONCLUSIONS

The direct simple shear test has near frictionless vertical boundaries that cannot develop complementary shear stresses necessary for *ideal* simple shear conditions. Simulations of the SGI type device using stacked rings demonstrate that the results compare well with *ideal* simple shear conditions for the expected range of soil-ring friction. Thus, current testing apparatuses are sufficient for approximating *ideal* simple shear conditions for the calibration of constitutive models. Increasing soil-ring friction increases the magnitude of stress non-uniformities that develop adjacent to the vertical boundaries during the consolidation phase and that in turn results in underestimating shear stresses during the shearing phase. Higher soil-ring friction did improve stress uniformity during the shearing phase, but the effect on consolidation stresses overwrite any advantages of having frictional vertical boundaries. Practically, near frictionless vertical boundaries achieve the best comparison with *ideal* simple shear conditions.

6 ACKNOWLEDGEMENTS

The authors would like to thank Rocscience Inc. and Klohn Crippen Berger for providing financial and technical support during the study. The authors also thank NSERC for Grant# 401267058 in support of the study. Without their help, the study would not have been possible.

7 REFERENCES

Airey, D.W., Budhu, M., and Wood, D.M. 1985. Some Aspects of the Behaviour of Soils in Simple Shear, *Developments in Soil Mechanics and Foundation Engineering: Vol. 2: Stress-Strain Modelling of Soils*, *Edited by* P. Banerjee, K. and R. Butterfield, Elsevier Applied Science Publishers, London, 2: 185-213.

Bernhardt, M.L., Biscontin, G., and O'Sullivan, C. 2016. Experimental validation study of 3D direct simple shear DEM simulations, *Soils and Foundations*, 56(3): 336-347.

Bjerrum, L., and Landva, A. 1966. Direct Simple-Shear Tests on a Norwegian Quick Clay, *Géotechnique*, 16(1): 1-20.

Chang, W.J., Phantachang, T., and Ieong, W.M. 2016. Evaluation of size and boundary effects in simple shear tests with distinct element modeling, *Journal of GeoEngineering*, 11(3): 133-142.

Dafalias, Y.F., and Manzari, M.T. 2004. Simple plasticity sand model accounting for fabric change effects, *Journal of Engineering Mechanics*, 130(6): 622-634.

Dassault Systèmes. 2012. ABAQUS Unified Finite Element Analysis, Vélizy-Villacoublay, France.

Doherty, J., and Fahey, M. 2011. Three-dimensional finite element analysis of the direct simple shear test, *Computers and Geotechnics*, 38: 917-924.

Gudehus, G., Amorosi, A., Gens, A., Herle, I., Kolymbas, D., Masin, D., Wood, D.M., Niemunis, A., Nova, R., Pastor, M., Tamagnini, C., and Viggiani, G. 2008. The soilmodels.info project, *International Journal of Numerical and Analytical Methods in Geomechanics*, 32(12): 1571-1572.

ITASCA Consulting Group Inc. 2019. FLAC3D Version 7.0 - Explicit continuum modeling of non-linear material behaviour in 3D, Minneapolis, USA.

Kjellman, W. 1951. Testing the Shear Strength of Clay in Sweden, *Géotechnique*, 2(3): 225-232.

Lucks, A.S., Christian, J.T., Brandow, G.E., and Höeg, K. 1972. Stress conditions in NGI simple shear test, *Journal of the Soil Mechanics and Foundations Division*, 98(1): 155-160.

Mao, X., and Fahey, M. 2003. Behaviour of calcareous soils in undrained cyclic simple shear, *Géotechnique*, 53(8): 715-727.

Masin, D., Martinelli, M., Miriano, C., and Tamagnini, C. 2018. SoilModels project - SANISAND Abaqus UMAT and Plaxis implementations, Available from https://soilmodels.com/download/plaxis-umat-sanisand/ [accessed May 29, 2018].

Niemunis, A. 2017. SoilModels project - Incremental Driver, Available from https://soilmodels.com/idriver/ [accessed May 29, 2018].

Rocscience Inc. 2019. RS3 - 3D finite element analysis for advanced analysis, Toronto, Canada.

Roscoe, K.H. 1953. An apparatus for the application of simple shear to soil samples, *3rd International Conference on Soil Mechanics and Foundation Engineering*, Zurich, Switzerland, 1: 186-191.

Saada, A.S., and Townsend, F.C. 1981. State of the Art: Labratory Strength Testing of Soils, *Laboratory Shear Strength of Soil, Edited by* R.N. Yong and F.C. Townsend, ASTM, STP 740: 7-77.

Shen, C.K., Sadigh, K., and Herrmann, L.R. 1978. An Analysis of NGI Simple Shear Apparatus for Cyclic Soil Testing, *Dynamic Geotechnical Testing, Edited by* M. Silver and D. Tiedemann, ASTM, STP 654: 148-162.

Taiebat, M., and Dafalias, Y.F. 2008. SANISAND: Simple anisotropic sand plasticity model, *International Journal for Numerical and Analytical Methods in Geomechanics*, 32(8): 915-948.

Tatsuoka, F., and Haibara, O. 1985. Shear resistance between sand and smooth or lubricated surfaces, *Soils and Foundations*, 25(1): 89-98.

Villet, W.C.B., Sitar, N., and Johnson, K.A. 1985. Simple shear tests on highly overconsolidated offshore silts, *17th Annual offshore technology conference*, OTC, Houston, Texas, USA, 1: 207-218.